Proton radioactivity in relativistic continuum Hartree-Bogoliubov theory

Yeunhwan Lim,[1,*] Xuewei Xia,[2,†] and Youngman Kim[1,‡]
[1]*Rare Isotope Science Project, Institute for Basic Science, Daejeon 305-811, Republic of Korea*
[2]*School of Physics and Nuclear Energy Engineering, Beihang University, Beijing 100191, China*
(Received 29 July 2015; revised manuscript received 24 November 2015; published 21 January 2016)

We investigate spherical proton emitters in the region from I ($Z = 53$) to Bi ($Z = 83$) isotopes as a crucial application of the relativistic energy density functional PC-PK1 beyond the drip line. The continuum effect is treated carefully by using the relativistic continuum Hartree-Bogoliubov theory. We calculate the half-lives of the proton emitters using the Wentzel-Kramers-Brillouin (WKB) method and observe that the calculated values are in reasonable agreement with experimental results for most of emitters considered in this study. We also discuss a clue to improve the functional PC-PK1 in future.

DOI: 10.1103/PhysRevC.93.014314

I. INTRODUCTION

The covariant density functional theory (CDFT) [1] has received much attention during the past decades due to its successful descriptions of lots of nuclear phenomena, not only in stable nuclei but also in exotic nuclei [2–4]. In particular, by taking the Lorentz symmetry into account, this covariant framework achieves a consistent treatment of the spin degrees of freedom [2,5], a natural origin of the pseudospin symmetry [6–9], and the unification of the time-even and time-odd components [10].

The traditional versions of CDFT are mainly based on the finite-range meson-exchange representation, such as density-dependent meson–nucleon couplings [11–13], in which the nucleus is described as a system of Dirac nucleons that interact with each other via the exchange of mesons and photons. More recently, this framework has been reinterpreted by the relativistic Kohn-Sham density functional theory, and the functionals have been developed based on the zero-range point-coupling interaction [14], in which the meson exchange in each channel is replaced by the corresponding local four-point contact interaction between nucleons. The point-coupling model has attracted more attention owing to the following advantages. First, it avoids the possible physical constrains introduced by explicit usage of the Klein-Gordon equation to describe meson fields, especially the fictitious σ meson. Second, it is possible to study the role of naturalness in effective theories for nuclear-structure-related problems [15]. Third, it is relatively easy to include the Fock terms [16], and provides more opportunities to investigate its relationship to the nonrelativistic approaches [17].

As one of the most successful relativistic point-coupling energy density functionals, PC-PK1 [18], whose parametrization is fitted to the binding energies, charge radii, and empirical pairing gaps of 60 selected spherical nuclei, has made great achievements in describing not only nuclear ground-state properties but also various excited-state properties. Representative examples include the studies of nuclear mass [19,20], neutron drip line [21], spin-orbit and orbit-orbit potential strengths [22], clustering structure [23], configuration mixing and low-lying excitations [24], collective Hamiltonian and shape phase transition [25], quadrupole [26] and magnetic [27] moments, magnetic [28] and antimagnetic [29] rotation bands, multiple chiral doublet bands [30], so-called stapler band [31], pairing transitions at finite temperature [32], exotic nuclear shape [33], fission barrier [34], shape coexistence and α decay [35], isoscalar proton-neutron pairing and β decay [36], and neutrinoless double-β decay [37]. With these successful applications, the energy density functional PC-PK1 is being used to construct one of the latest versions of CDFT nuclear mass table, where a proper treatment of pairing correlations in the presence of the continuum can be achieved within the framework of relativistic continuum Hartree-Bogoliubov (RCHB) theory [4,38–41]. It is found that the couplings between the bound states and the continuum due to the pairing correlation strongly affect the drip-line position. By comparison with the finite-range droplet model, the neutron drip-line nucleus predicted by the RCHB theory with PC-PK1 functional has 2 (O), 10 (Ne), 10 (Na), 6 (Mg), 8 (Al), 6 (Si), 8 (P), 6 (S), 14 (K), 10 (Ca), 10 (Sc), and 12 (Ti) more neutrons, respectively [42].

The study of exotic nuclei in which many novel phenomena has been observed and predicted, such as the change of magic number, giant halo [43,44], and shape decoupling between core and halo [45], is an indispensable component of contemporary nuclear physics. In particular, exotic nuclei beyond the drip lines pose great challenges in both experimental and theoretical researches. The proton radioactivity from proton rich nuclei beyond the drip line provides not only spectroscopic information on nuclear structures but also invaluable clues on the nuclear force beyond the drip line. These proton emitters are also interesting open systems for quantum mechanical tunneling as the emitted proton goes through the barrier of Coulomb and centrifugal potentials. Experimentally, an isomeric state of ^{53}Co* was discovered as the first proton emitter in 1970 [46,47]. Since then more than 30 proton emitters have been observed, mainly in the region from I ($Z = 53$) to Bi ($Z = 83$) isotopes; see, e.g., Refs. [48,49] and the references therein. To understand the physics beyond the drip line, comprehensive theoretical efforts have been

*ylim9057@ibs.re.kr
†xiaxw1230@gmail.com
‡ykim@ibs.re.kr

made [50–54]. Recently, the proton emission half-lives were systematically investigated in the framework of CDFT [55,56].

In this work, as another crucial application of the relativistic energy density functional PC-PK1 beyond the drip line, we will systematically study the properties of (near) spherical proton emitters in the region from I ($Z = 53$) to Bi ($Z = 83$) isotopes. The continuum effect is treated carefully by using the RCHB [4] framework, and the numerical setup is the same as that used in the latest CDFT mass table [42] without any additional parameter.

This paper is organized as follows. In Sec. II, the covariant density functional theory and its Bogoliubov transformation are explained briefly. We account for the Wentzel-Kramers-Brillouin (WKB) approximation for proton emission half-lives in Sec. III. Section IV summarizes and discusses the results of the present work.

II. COVARIANT DENSITY FUNCTIONAL THEORY

The starting point of the point-coupling CDFT is an effective Lagrangian density [18]

$$\begin{aligned}\mathcal{L} = {} & \bar{\psi}(i\gamma_\mu\partial^\mu - M)\psi - \frac{1}{4}F_{\mu\nu}F^{\mu\nu} - e\frac{1-\tau_3}{2}\bar{\psi}\gamma^\mu\psi A_\mu \\ & - \frac{1}{2}\alpha_S(\bar{\psi}\psi)(\bar{\psi}\psi) - \frac{1}{2}\alpha_V(\bar{\psi}\gamma_\mu\psi)(\bar{\psi}\gamma^\mu\psi) \\ & - \frac{1}{2}\alpha_{TV}(\bar{\psi}\vec{\tau}\gamma_\mu\psi)(\bar{\psi}\vec{\tau}\gamma^\mu\psi) - \frac{1}{2}\alpha_{TS}(\bar{\psi}\vec{\tau}\psi)(\bar{\psi}\vec{\tau}\psi) \\ & - \frac{1}{3}\beta_S(\bar{\psi}\psi)^3 - \frac{1}{4}\gamma_S(\bar{\psi}\psi)^4 - \frac{1}{4}\gamma_V[(\bar{\psi}\gamma_\mu\psi\psi)(\bar{\psi}\gamma^\mu\psi)]^2 \\ & - \frac{1}{2}\delta_S\partial_\nu(\bar{\psi}\psi)\partial^\nu(\bar{\psi}\psi) - \frac{1}{2}\delta_V\partial_\nu(\bar{\psi}\gamma_\mu\psi)\partial^\nu(\bar{\psi}\gamma^\mu\psi) \\ & - \frac{1}{2}\delta_{TV}\partial_\nu(\bar{\psi}\vec{\tau}\gamma_\mu\psi)\partial^\nu(\bar{\psi}\vec{\tau}\gamma^\mu\psi) \\ & - \frac{1}{2}\delta_{TS}\partial_\nu(\bar{\psi}\vec{\tau}\psi)\partial^\nu(\bar{\psi}\vec{\tau}\psi), \end{aligned} \tag{1}$$

where M is the nucleon mass, A_μ and $F^{\mu\nu}$ are for photon fields, and α_S, α_V, α_{TV}, α_{TS}, β_S, γ_S, γ_V, δ_S, δ_V, δ_{TV}, and δ_{TS} are the coupling constants in different spin-isospin channels. In this paper, we adopt the natural units $\hbar = c = 1$.

From the above Lagrangian density, we derive the RCHB equation [4]

$$\begin{pmatrix} h_D - \lambda & \Delta \\ -\Delta^* & -h_D^* + \lambda \end{pmatrix}\begin{pmatrix} U_k \\ V_k \end{pmatrix} = E_k\begin{pmatrix} U_k \\ V_k \end{pmatrix}, \tag{2}$$

where λ is the Fermi energy and E_k are the eigenenergies of quasiparticles. The Dirac Hamiltonian h_D is given by

$$h_D = \boldsymbol{\alpha}\cdot\mathbf{p} + \beta[M + S(\mathbf{r})] + V(\mathbf{r}), \tag{3}$$

where the scalar $S(\mathbf{r})$ and vector $V(\mathbf{r})$ potentials are

$$\begin{aligned} S(\mathbf{r}) &= \alpha_S\rho_S + \beta_S\rho_S^2 + \gamma_S\rho_S^3 + \delta_S\Delta\rho_S, \\ V(\mathbf{r}) &= \alpha_V\rho_V + \gamma_V\rho_V^3 + \delta_V\Delta\rho_V + eA_0 \\ &\quad + \alpha_{TV}\tau_3\rho_{TV} + \delta_{TV}\tau_3\Delta\rho_{TV}. \end{aligned} \tag{4}$$

TABLE I. Parameters in PC-PK1 and pairing strength

	Value	Dimension
m_n	939	MeV
m_p	939	MeV
α_S	-3.96291×10^{-4}	MeV^{-2}
β_S	8.6653×10^{-1}	MeV^{-5}
γ_S	-3.80724×10^{-17}	MeV^{-8}
δ_S	-1.09108×10^{-10}	MeV^{-4}
α_V	2.6904×10^{-4}	MeV^{-2}
γ_V	-3.64219×10^{-18}	MeV^{-8}
δ_V	-4.32619×10^{-10}	MeV^{-4}
α_{TV}	2.95018×10^{-5}	MeV^{-2}
δ_{TV}	-4.11112×10^{-10}	MeV^{-4}
V_0	685	MeV fm^{-3}

The scalar, vector, and isospin densities are expressed as

$$\begin{aligned} \rho_S(\mathbf{r}) &= \sum_k \overline{V}_k(\mathbf{r})V_k(\mathbf{r}), \\ \rho_V(\mathbf{r}) &= \sum_k V_k^\dagger(\mathbf{r})V_k(\mathbf{r}), \\ \rho_{TV}(\mathbf{r}) &= \sum_k V_k^\dagger(\mathbf{r})\tau_3 V_k(\mathbf{r}). \end{aligned} \tag{5}$$

The pairing gap takes the form of

$$\Delta_{kk'}(\mathbf{r},\mathbf{r}') = -\sum_{\tilde{k}\tilde{k}'} V_{kk',\tilde{k}\tilde{k}'}(\mathbf{r},\mathbf{r}')\kappa_{kk'}(\mathbf{r},\mathbf{r}'), \tag{6}$$

where $\kappa = U^*V^T$ is the pairing tensor. For $V_{kk',\tilde{k}\tilde{k}'}$ the following density-dependent zero-range pairing force is adopted:

$$V^{pp}(\mathbf{r}_1,\mathbf{r}_2) = -V_0\delta(\mathbf{r}_1 - \mathbf{r}_2)\frac{1}{4}(1 - P^\sigma)\left(1 - \frac{\rho(\mathbf{r}_1)}{\rho_0}\right), \tag{7}$$

where P^σ is the spin exchange operator and $\rho_0 = 0.152\ \text{fm}^{-3}$.

By representing the single-particle levels in the canonical basis [57], we can obtain the occupation probability v^2 and nonoccupation probability u^2 in the BCS-like form for each orbital. The latter plays a very important role in calculating the spectroscopic factor of proton emission. Table I shows the masses of proton and neutron, coupling constants, and pairing strength used in this work.

III. WKB APPROXIMATION FOR PROTON EMISSIONS

In order to calculate proton emission half-lives, we adopt the traditional Wentzel-Kramers-Brillouin (WKB) method. In this method, the decay width is given by

$$\Gamma = \frac{S\mathcal{N}}{4\mu}\exp\left[-2\int_{r_1}^{r_2}|k(r)|dr\right], \tag{8}$$

where S is the spectroscopic factor, $\mathcal{N}$ is the normalization factor, r_1 and r_2 are the classical turning points for the emitted proton, and $k(r) = \sqrt{2\mu[E - V(r)]}$. Here we take E as the experimental Q value. Within a two-body scheme, the emitted proton penetrates the potential barrier provided by the daughter

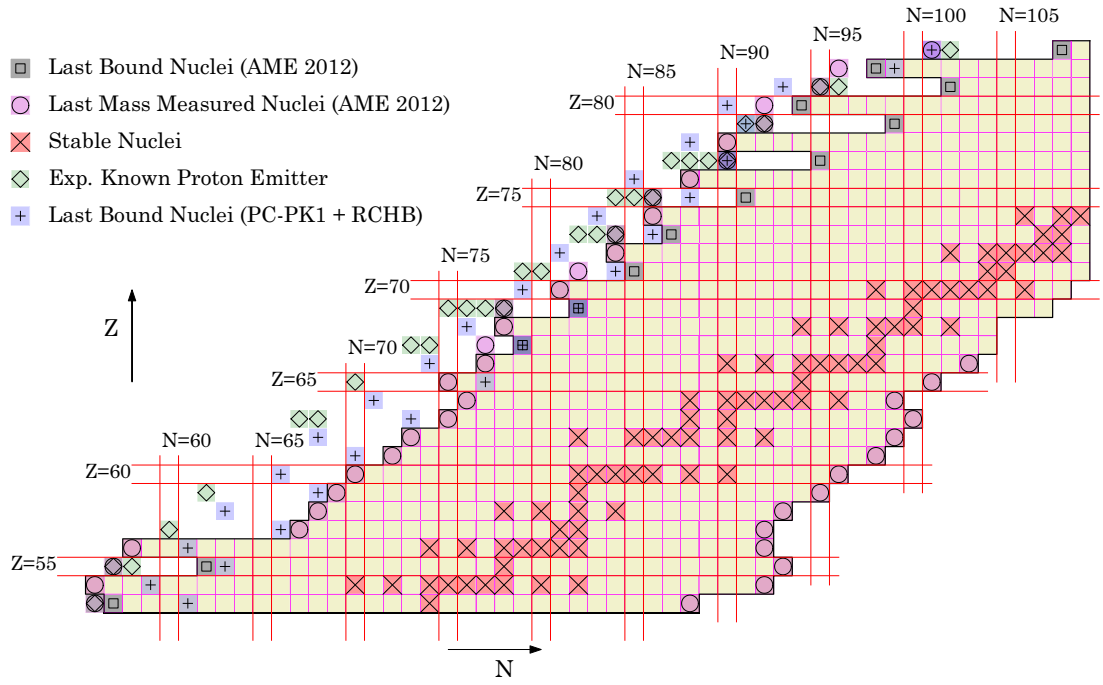

FIG. 1. Partial nuclear chart from I ($Z = 53$) to Bi ($Z = 83$) isotopes by the RCHB theory with the covariant density functional PC-PK1. The experimentally known proton emitters [48] are denoted with the symbol $\diamond$, while the proton drip-line nuclei given by the spherical RCHB calculations with relativistic density functional PC-PK1 [18] and pairing strength $V_0 = 685$ MeV fm^{-3} are shown with the symbol $+$. The stable nuclei as well as the last mass-measured nuclei and the last bound nuclei in AME 2012 [59] are also shown for guiding eyes.

nucleus, and therefore μ represents the reduced mass, $\mu = M(A-1)/A$.

The potential barrier $V(r)$ includes the nuclear, Coulomb, and centrifugal contributions

$$V(r) = V_N(r) + V_C(r) + \frac{\hbar^2}{2\mu r^2} l(l+1). \tag{9}$$

Here $V_N(r) = V(r) + S(r)$ and $V_C(r)$ are the nuclear and Coulomb potentials for the protons, which are calculated self-consistently by the RCHB theory with the PC-PK1 functional. Moreover, the spectroscopic factor S in Eq. (8) is obtained within the same self-consistent scheme; i.e., S is the nonoccupation probability u^2 in the canonical basis for the specific orbital in the daughter nucleus, $S = u^2$. The last term is the contribution from the centrifugal barrier. We used the traditional centrifugal barrier instead of the Langer modified centrifugal barrier [58]. We found that there is less than 5% difference in numerical calculation between the Langer centrifugal barrier [$V_l = \frac{\hbar^2}{2\mu r^2}(l+1/2)^2$] and the traditional one if $l \neq 0$. However, the discrepancies become more than 20% in some cases with $l = 0$ because of the first classical turning point.

Furthermore, the normalization factor, which is responsible for the assaulting frequencies, is calculated by [58]

$$\frac{1}{\mathcal{N}} = \int_{r_0}^{r_1} \frac{dr}{k(r)} \cos^2\left[\int_{r_0}^{r} k(r')dr' - \frac{\pi}{4}\right]. \tag{10}$$

With all of the above ingredients, the proton emission half-lives read

$$t_{1/2} = \frac{\ln 2}{\Gamma}. \tag{11}$$

Note that compared with the formalism used in Ref. [56], we took into account only the leading-order contribution of the

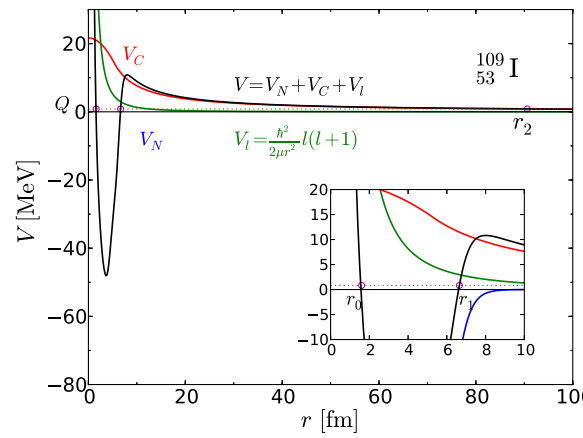

FIG. 2. Potential barrier for the proton emission of ^{109}I. The nuclear V_N and Coulomb V_C potentials are obtained from the mother nucleus, while the Q value (dotted line) is taken as the experimental value. The r_0, r_1, and r_2 are classical turning points of the potential barrier for the emitted proton.

TABLE II. Calculated and experimental half-lives of (near) spherical proton emitters from I ($Z = 53$) to Bi ($Z = 83$), where asterisk ($*$) denotes the isomeric states. The Q values from experiments, single-particle orbitals, and half-lives are taken from Ref. [48] with the updates for $^{156}_{73}$Ta and $^{160}_{75}$Re from Refs. [60,61]. The nonoccupation probabilities u^2 of the corresponding orbital in the daughter nucleus are calculated by the RCHB theory with PC-PK1 functional. The BCS results are shown in the parentheses next to the RCHB results. For comparison, the calculated one-proton separation energies S_p are also shown.

No.	Nucleus	$-S_p$ (MeV)	Q (MeV)	Orbital	u^2	$t^{\rm th}_{1/2}$	$t^{\rm exp}_{1/2}$
1	$^{109}_{53}$I	2.20	0.827(5)	$2d_{5/2}$	0.9233 (0.9246)	36.18 (33.14) μs	93.5(5) μs
2	$^{112}_{55}$Cs	2.42	0.823(7)	$2d_{5/2}$	0.8744 (0.9067)	0.23 (0.21) ms	0.5(1) ms
3	$^{113}_{55}$Cs	1.97	0.976(3)	$2d_{5/2}$	0.8811 (0.9185)	1.74 (1.56) μs	16.7(7) μs
4	$^{144}_{69}$Tm	1.85	1.725(16)	$1h_{11/2}$	0.7451 (0.8138)	4.84 (4.21) μs	$2.7^{+1.7}_{-0.7}$ μs
5	$^{145}_{69}$Tm	1.55	1.753(7)	$1h_{11/2}$	0.7376 (0.8013)	3.07 (2.70) μs	3.46(32) μs
6	$^{146}_{69}$Tm	1.23	1.210(4)	$1h_{11/2}$	0.7240 (0.7884)	129.63 (112.59) ms	117.6(64) ms
7	$^{146}_{69}$Tm*		1.140(4)	$1h_{11/2}$	0.7240 (0.7884)	866.47 (751.66) ms	203(6) ms
8	$^{147}_{69}$Tm	0.95	1.073(5)	$1h_{11/2}$	0.7209 (0.7779)	6.08 (5.35) s	3.78(127) s
9	$^{147}_{69}$Tm*		1.133(3)	$2d_{3/2}$	0.6546 (0.6432)	627.26 (602.20) μs	360(36) μs
10	$^{150}_{71}$Lu	1.31	1.283(3)	$1h_{11/2}$	0.6076 (0.6558)	88.46 (77.58) ms	64.0(56) ms
11	$^{150}_{71}$Lu*		1.306(5)	$2d_{3/2}$	0.5524 (0.5381)	35.72 (34.15) μs	43^{+7}_{-5} μs
12	$^{151}_{71}$Lu	1.03	1.253(3)	$1h_{11/2}$	0.6098 (0.6434)	176.38 (159.66) ms	127.1(18) ms
13	$^{151}_{71}$Lu*		1.332(10)	$2d_{3/2}$	0.5786 (0.5755)	18.03 (17.21) μs	16(1) μs
14	$^{155}_{73}$Ta	1.08	1.468(15)	$1h_{11/2}$	0.4955 (0.5036)	5.25 (4.98) ms	$2.9^{+1.5}_{-1.1}$ ms
15	$^{156}_{73}$Ta	0.76	1.032(5)	$2d_{3/2}$	0.5339 (0.5328)	338.86 (321.00) ms	149(8) ms
16	$^{156}_{73}$Ta*		1.127(7)	$1h_{11/2}$	0.4836 (0.5032)	25.37 (23.40) s	8.52(212) s
17	$^{157}_{73}$Ta	0.46	0.947(7)	$3s_{1/2}$	0.7131 (0.7838)	1117.50 (957.80) ms	300(105) ms
18	$^{159}_{75}$Re*		1.831(20)	$1h_{11/2}$	0.3829 (0.3783)	31.14 (30.54) μs	20.2(37) μs
19	$^{160}_{75}$Re	0.74	1.287(6)	$2d_{3/2}$	0.4481 (0.4568)	0.91 (0.85) ms	0.687(11) ms
20	$^{161}_{75}$Re	0.45	1.214(6)	$3s_{1/2}$	0.6774 (0.7715)	844.90 (705.15) μs	440(2) μs
21	$^{161}_{75}$Re*		1.338(7)	$1h_{11/2}$	0.3696 (0.3541)	367.72 (370.29) ms	224(31) ms
22	$^{164}_{77}$Ir*		1.844(9)	$1h_{11/2}$	0.2508 (0.2287)	96.51 (103.08) μs	113^{+62}_{-30} μs
23	$^{165}_{77}$Ir*		1.733(7)	$1h_{11/2}$	0.2489 (0.2143)	0.55 (0.62) ms	0.34(7) ms
24	$^{166}_{77}$Ir	0.07	1.168(7)	$2d_{3/2}$	0.3854 (0.4492)	105.57 (85.96) ms	152(71) ms
25	$^{166}_{77}$Ir*		1.340(8)	$1h_{11/2}$	0.2359 (0.2001)	1.71 (1.94) s	840(280) ms
26	$^{167}_{77}$Ir	-0.21	1.096(6)	$3s_{1/2}$	0.6778 (0.7921)	120.38 (97.87) ms	110(15) ms
27	$^{167}_{77}$Ir*		1.261(7)	$1h_{11/2}$	0.2345 (0.1868)	12.69 (15.28) s	7.5(24) s
28	$^{170}_{79}$Au	-0.03	1.488(12)	$2d_{3/2}$	0.2701 (0.3037)	169.40 (144.46) μs	321^{+67}_{-58} μs
29	$^{170}_{79}$Au*		1.770(6)	$1h_{11/2}$	0.1262 (0.1008)	1.50 (1.82) ms	$1.046^{+0.136}_{-0.126}$ ms
30	$^{171}_{79}$Au	-0.29	1.464(10)	$3s_{1/2}$	0.6467 (0.7253)	26.20 (22.36) μs	$24.5^{+4.7}_{-3.1}$ μs
31	$^{171}_{79}$Au*		1.719(4)	$1h_{11/2}$	0.1243 (0.0963)	3.50 (4.34) ms	2.22(19) ms
32	$^{176}_{81}$Tl	-0.80	1.282(18)	$3s_{1/2}$	0.5811 (0.4950)	8.73 (9.68) ms	$5.2^{+3.0}_{-1.4}$ ms
33	$^{177}_{81}$Tl	-1.07	1.180(20)	$3s_{1/2}$	0.5887 (0.5018)	163.34 (180.03) ms	67(37) ms
34	$^{177}_{81}$Tl*		1.984(8)	$1h_{11/2}$	0.0406 (0.0513)	380.60 (288.24) μs	396^{+87}_{-77} μs
35	$^{185}_{83}$Bi	-2.01	1.624(16)	$4s_{1/2}$	1.0000 (1.0000)	5.79 (5.48) μs	58(9) μs

nuclear potential from the point of view of similarity renormalization group. However, here we perform self-consistent calculations without any additional free parameters, so that the predictive power of a given nuclear energy density functional can be examined in a more strict way.

IV. RESULTS AND DISCUSSION

In Fig. 1 the nuclear chart from the I ($Z = 53$) to Bi ($Z = 83$) isotopes is shown, where the experimentally known proton emitters [48] are highlighted with $\diamond$ symbols. The proton

drip-line nuclei given by the spherical RCHB calculations with the relativistic energy density functional PC-PK1 [18] and pairing strength $V_0 = 685$ MeV fm^{-3} [42] are compared with the last bound or last mass-measured nuclei in AME 2012 [59].

Experimentally, the possible candidates of proton emitters should be located outside the proton drip line with positive Q values. The corresponding conditions for the calculated results are $S_p > 0$, $S_{2p} > 0$, and $\lambda_p < 0$, where S_p and S_{2p} are the one- and two-proton separation energies, respectively, and λ_p is the Fermi energy. For the proton emitters discovered in this region it is found that the above conditions are well satisfied by the self-consistent RCHB calculations in the whole region, except for a few cases with $A > 167$.

By taking the proton emitter ^{109}I as an example, Fig. 2 shows the nuclear, Coulomb, and centrifugal contributions to the potential barrier $V(r)$ in Eq. (9), which are short, long, and medium range, respectively. The classical turning point r_0 close to the center of the nucleus is mainly decided by the centrifugal barrier, while the turning point r_2 far away from the center is mainly decided by the Coulomb potential. In contrast, the turning point r_1 near the nuclear surface is a result of the competition among all contributions. It is noteworthy to mention the differences between the traditional centrifugal barrier and the Langer potential [58]. Using the Langer potential, the first classical turning point (r_0) is always located away from the center even with $l = 0$. Because of this fact, WKB calculation from the Langer potential with $l = 0$ underestimates the half-lives compared with the result from the traditional centrifugal barrier contribution. This is caused by the assaulting frequencies from the Langer potential is higher than the traditional one. If $l \neq 0$, however, the half-lives are overestimated since the penetration length $(r_2 - r_1)$ is increased.

In Table II, we summarize the calculated and experimental half-lives of (near) spherical proton emitters from I ($Z = 53$) to Bi ($Z = 83$), where asterisk ($*$) denotes the isomeric states. As shown in Table II, the calculated one-proton separation energies are still not accurate enough for describing the Q values of proton emission, thus here we adopt the experiment Q values taken from Ref. [48]. The experimental values are also taken for the single-particle orbitals. Meanwhile, the calculated nuclear and Coulomb potentials are used to obtain the normalization factor in Eq. (10) and decay width in Eq. (8), together with the spectroscopic factor S as the nonoccupation probabilities u^2 of the corresponding orbital in the daughter nucleus. The proton emission phenomena of the ground and isomeric states indicate that the nuclear potentials for protons from both states are quite similar to each other. For example, two types of proton emissions were experimentally observed in $^{155}_{71}$Lu. The half-lives of the observed proton emission, however, are different in four orders of magnitude. Considering spectroscopic factor and experimental Q values, the difference comes mainly from the centrifugal potentials. This suggests that the proton emission from the both states highly depends on the angular momentum of the emitted proton. This justifies the use of nuclear potential obtained from the ground state for the isomeric states. We also performed the same calculation with BCS formalism. In the proton-dripline region, the pairing effects is less important than the neutron-rich nuclei since the Coulomb repulsion is the main reason of disintegration of proton-rich nuclei. The numerical number in the parentheses next to RCHB results in Table II shows the BCS results. There are slight differences in u^2 between BCS and RCHB results. The half-lives from RCHB, however, give better agreement as the number of nucleon in nuclei increases in which pairing and continuum effects are getting important.

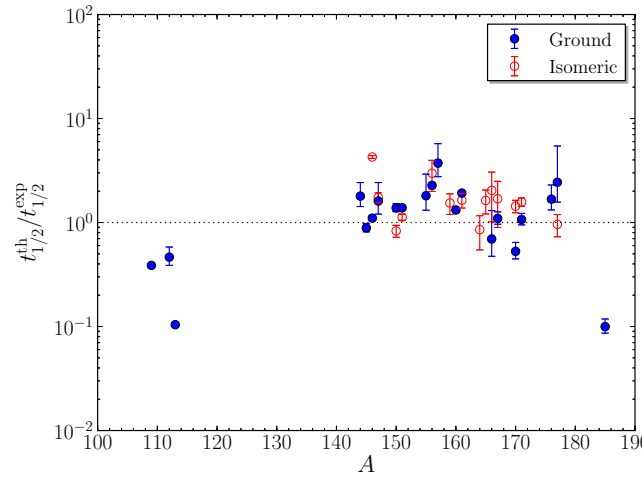

FIG. 3. Ratios of the calculated half-lives $t^{th}_{1/2}$ to experimental half-lives $t^{exp}_{1/2}$ [48,60,61] as a function of mass number A, where the error bars indicate the uncertainties of the experiment values, $\delta t^{exp}_{1/2}/t^{exp}_{1/2}$. The proton emissions from the ground states and isomeric states are denoted with solid (blue online) and open (red online) symbols, respectively.

It is seen that the proton emission half-lives range from a few microseconds to a few seconds, which are mainly determined by the orbital angular momentum and Q value. For all the cases covering six orders of magnitude, the theoretical results by the relativistic energy density functional PC-PK1 are in good agreement with the experimental data, without a single adjustable parameter. This can be seen more clearly in Fig. 3, in which the ratios of the calculated half-lives $t^{th}_{1/2}$ to experimental half-lives $t^{exp}_{1/2}$ are shown as a function of mass number A. The solid (blue online) and open (red online) symbols represent the proton emissions from the ground states and isomeric states, respectively, and the error bars indicate the uncertainties of the experiment values, $\delta t^{exp}_{1/2}/t^{exp}_{1/2}$. It is found that for the nuclei $^{113}_{55}$Cs and $^{185}_{83}$Bi, the results underestimate the data by around one order of magnitude and for the others, the calculated half-lives $t^{th}_{1/2}$ reproduce the data within a factor of 4 and many of them even within a factor of 2.

On one hand, the reasonably nice results on the proton emission half-lives indicate that, by treating properly the pairing correlations in the presence of the continuum within the framework of RCHB theory, the relativistic energy density functional PC-PK1 describes very well the mean-field potentials and the (non)occupation probabilities, even beyond the proton drip line.

On the other hand, although the ratios $t^{th}_{1/2}/t^{exp}_{1/2}$ in Fig. 3 do not show a systematic deviation as a function A when

the experimental Q values are adopted, it is not the case if the calculated one-proton separation energies S_p are adopted instead. In the region from I to Bi, it is found that the $-S_p$ overestimates the Q value when A is small and underestimates the Q value with larger A. This systematic deviation will be one of the guidelines for further improvement of the functional PC-PK1 in future.

ACKNOWLEDGMENTS

We acknowledge the fruitful discussions with Ying Chen, Haozhao Liang, Jie Meng, Shuangquan Zhang, and Shan-Gui Zhou. The work of Y.L. and Y.K. was supported by the Rare Isotope Science Project of Institute for Basic Science funded by Ministry of Science, ICT and Future Planning and National Research Foundation of Korea (2013M7A1A1075764).

[1] B. D. Serot and J. D. Walecka, *Advances in Nuclear Physics Vol. 16: The Relativistic Nuclear Many Body Problem*, edited by J. W. Negele and E. Vogt (Plenum Press, New York, 1986).
[2] P. Ring, Prog. Part. Nucl. Phys. **37**, 193 (1996).
[3] D. Vretenar, A. V. Afanasjev, G. A. Lalazissis, and P. Ring, Phys. Rep. **409**, 101 (2005).
[4] J. Meng, H. Toki, S. G. Zhou, S. Q. Zhang, W. H. Long, and L. S. Geng, Prog. Part. Nucl. Phys. **57**, 470 (2006).
[5] S.-G. Zhou, J. Meng, and P. Ring, Phys. Rev. Lett. **91**, 262501 (2003).
[6] J. Meng, K. Sugawara-Tanabe, S. Yamaji, P. Ring, and A. Arima, Phys. Rev. C **58**, R628 (1998).
[7] J. Meng, K. Sugawara-Tanabe, S. Yamaji, and A. Arima, Phys. Rev. C **59**, 154 (1999).
[8] T. S. Chen, H. F. Lu, J. Meng, S. Q. Zhang, and S.-G. Zhou, Chin. Phys. Lett. **20**, 358 (2003).
[9] H. Liang, J. Meng, and S.-G. Zhou, Phys. Rep. **570**, 1 (2015).
[10] J. Meng, J. Peng, S. Q. Zhang, and P. W. Zhao, Front. Phys. **8**, 55 (2013).
[11] W. H. Long, J. Meng, N. Van Giai, and S.-G. Zhou, Phys. Rev. C **69**, 034319 (2004).
[12] W. H. Long, N. Van Giai, and J. Meng, Phys. Lett. B **640**, 150 (2006).
[13] W. H. Long, H. Sagawa, N. Van Giai, and J. Meng, Phys. Rev. C **76**, 034314 (2007).
[14] B. A. Nikolaus, T. Hoch, and D. G. Madland, Phys. Rev. C **46**, 1757 (1992).
[15] T. Bürvenich, D. G. Madland, J. A. Maruhn, and P.-G. Reinhard, Phys. Rev. C **65**, 044308 (2002).
[16] H. Liang, P. W. Zhao, P. Ring, X. Roca-Maza, and J. Meng, Phys. Rev. C **86**, 021302(R) (2012).
[17] A. Sulaksono, T. Bürvenich, J. A. Maruhn, P. G. Reinhard, and W. Greiner, Ann. Phys. **308**, 354 (2003).
[18] P. W. Zhao, Z. P. Li, J. M. Yao, and J. Meng, Phys. Rev. C **82**, 054319 (2010).
[19] P. W. Zhao, L. S. Song, B. Sun, H. Geissel, and J. Meng, Phys. Rev. C **86**, 064324 (2012).
[20] K. Q. Lu, Z. X. Li, Z. P. Li, J. M. Yao, and J. Meng, Phys. Rev. C **91**, 027304 (2015).
[21] A. V. Afanasjev, S. E. Agbemava, D. Ray, and P. Ring, Phys. Rev. C **91**, 014324 (2015).
[22] H. Liang, P. Zhao, L. Li, and J. Meng, Phys. Rev. C **83**, 011302(R) (2011).
[23] J. M. Yao, N. Itagaki, and J. Meng, Phys. Rev. C **90**, 054307 (2014).
[24] J. M. Yao, K. Hagino, Z. P. Li, J. Meng, and P. Ring, Phys. Rev. C **89**, 054306 (2014).
[25] Z. H. Wang, J. Xiang, W. H. Long, and Z. P. Li, J. Phys. G: Nucl. Part. Phys. **42**, 045108 (2015).
[26] P. W. Zhao, S. Q. Zhang, and J. Meng, Phys. Rev. C **89**, 011301(R) (2014).
[27] J. Li, J. X. Wei, J. N. Hu, P. Ring, and J. Meng, Phys. Rev. C **88**, 064307 (2013).
[28] L. F. Yu, P. W. Zhao, S. Q. Zhang, P. Ring, and J. Meng, Phys. Rev. C **85**, 024318 (2012).
[29] J. Peng and P. W. Zhao, Phys. Rev. C **91**, 044329 (2015).
[30] I. Kuti *et al.*, Phys. Rev. Lett. **113**, 032501 (2014).
[31] Z. Q. Chen, S. Y. Wang, L. Liu, P. Zhang, H. Jia, B. Qi, S. Wang, D. P. Sun, C. Liu, Z. Q. Li, X. G. Wu, G. S. Li, C. Y. He, Y. Zheng, and L. H. Zhu, Phys. Rev. C **91**, 044303 (2015).
[32] Y. F. Niu, Z. M. Niu, N. Paar, D. Vretenar, G. H. Wang, J. S. Bai, and J. Meng, Phys. Rev. C **88**, 034308 (2013).
[33] J. Zhao, B.-N. Lu, E.-G. Zhao, and S.-G. Zhou, Phys. Rev. C **86**, 057304 (2012).
[34] B.-N. Lu, E.-G. Zhao, and S.-G. Zhou, Phys. Rev. C **85**, 011301(R) (2012).
[35] Z. X. Li, Z. H. Zhang, and P. W. Zhao, Front. Phys. **10**, 102101 (2015).
[36] Z. M. Niu, Y. F. Niu, Q. Liu, H. Z. Liang, and J. Y. Guo, Phys. Rev. C **87**, 051303(R) (2013).
[37] L. S. Song, J. M. Yao, P. Ring, and J. Meng, Phys. Rev. C **90**, 054309 (2014).
[38] J. Meng and P. Ring, Phys. Rev. Lett. **77**, 3963 (1996).
[39] J. Meng, Nucl. Phys. A **635**, 3 (1998).
[40] W. Zhang, J. Meng, S. Zhang, L. Geng, and H. Toki, Nucl. Phys. A **753**, 106 (2005).
[41] J. Meng and S.-G. Zhou, J. Phys. G **42**, 093101 (2015).
[42] X. Y. Qu, Y. Chen, S. Q. Zhang, P. W. Zhao, I. Shin, Y. Lim, Y. Kim, and J. Meng, Sci. China Phys. Mech. Astron. **56**, 2031 (2013).
[43] J. Meng and P. Ring, Phys. Rev. Lett. **80**, 460 (1998).
[44] J. Meng, H. Toki, J. Y. Zeng, S. Q. Zhang, and S.-G. Zhou, Phys. Rev. C **65**, 041302 (2002).
[45] S.-G. Zhou, J. Meng, P. Ring, and E.-G. Zhao, Phys. Rev. C **82**, 011301 (2010).
[46] K. P. Jackson, C. U. Cardinal, H. C. Evans, N. A. Jelley, and J. Cerny, Phys. Lett. B **33**, 281 (1970).
[47] J. Cerny, J. E. Esterl, R. A. Gough, and R. G. Sextro, Phys. Lett. B **33**, 284 (1970).
[48] B. Blank and M. Borge, Prog. Part. Nucl. Phys. **60**, 403 (2008).
[49] M. Pfützner, M. Karny, L. V. Grigorenko, and K. Riisager, Rev. Mod. Phys. **84**, 567 (2012).
[50] S. Åberg, P. B. Semmes, and W. Nazarewicz, Phys. Rev. C **56**, 1762 (1997); **58**, 3011(E) (1998).
[51] E. Maglione, L. S. Ferreira, and R. J. Liotta, Phys. Rev. Lett. **81**, 538 (1998).

[52] G. A. Lalazissis, D. Vretenar, and P. Ring, Nucl. Phys. A **650**, 133 (1999).
[53] D. Vretenar, G. A. Lalazissis, and P. Ring, Phys. Rev. Lett. **82**, 4595 (1999).
[54] H. Esbensen and C. N. Davids, Phys. Rev. C **63**, 014315 (2000).
[55] L. Ferreira, E. Maglione, and P. Ring, Phys. Lett. B **701**, 508 (2011).
[56] Q. Zhao, J. M. Dong, J. L. Song, and W. H. Long, Phys. Rev. C **90**, 054326 (2014).
[57] P. Ring and P. Schuck, *The Nuclear Many-Body Problem* (Springer-Verlag, New York, 1980).
[58] B. Buck, A. C. Merchant, and S. M. Perez, Phys. Rev. C **45**, 1688 (1992).
[59] M. Wang, G. Audi, A. H. Wapstra, F. G. Kondev, M. MacCormick, X. Xu, and B. Pfeiffer, Chin. Phys. C **36**, 1603 (2012).
[60] I. Darby *et al.*, Phys. Rev. C **83**, 064320 (2011).
[61] C. Qi, D. S. Delion, R. J. Liotta, and R. Wyss, Phys. Rev. C **85**, 011303(R) (2012).